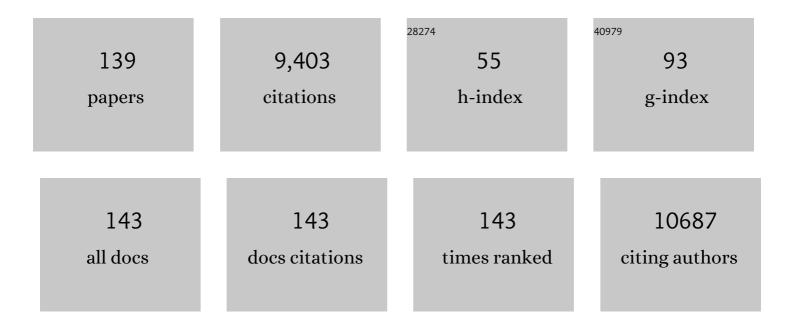
List of Publications by Year in descending order

Source: https://exaly.com/author-pdf/4155527/publications.pdf Version: 2024-02-01



#	Article	IF	CITATIONS
1	Low-crystalline PdCu alloy on large-area ultrathin 2D carbon nitride nanosheets for efficient photocatalytic Suzuki coupling. Applied Catalysis B: Environmental, 2022, 300, 120756.	20.2	29
2	Plasma-assisted in-situ preparation of graphene-Ag nanofiltration membranes for efficient removal of heavy metal ions. Journal of Hazardous Materials, 2022, 423, 127012.	12.4	29
3	Freestanding N-doped graphene membrane electrode with interconnected porous architecture for efficient capacitive deionization. Carbon, 2022, 187, 86-96.	10.3	39
4	Molecular Dipoleâ€Induced Photoredox Catalysis for Hydrogen Evolution over Selfâ€Assembled Naphthalimide Nanoribbons. Angewandte Chemie, 2022, 134, .	2.0	7
5	Super-hydrophobic and photocatalytic antimicrobial activity of iodine-doped ZnO nanoarray films. New Journal of Chemistry, 2022, 46, 3140-3145.	2.8	6
6	Molecular Dipoleâ€Induced Photoredox Catalysis for Hydrogen Evolution over Selfâ€Assembled Naphthalimide Nanoribbons. Angewandte Chemie - International Edition, 2022, 61, .	13.8	31
7	In-situ Formed Surface Complexes Promoting NIR-Light-Driven Carbonylation of Diamine with CO on Ultrathin Co2CO3(OH)2 Nanosheets. Applied Catalysis B: Environmental, 2022, 306, 121103.	20.2	6
8	Solar Photocatalytic Oxidation of Methane to Methanol with Water over RuO _{<i>x</i>} /ZnO/CeO ₂ Nanorods. ACS Sustainable Chemistry and Engineering, 2022, 10, 16-22.	6.7	30
9	Solar-to-Chemical Fuel Conversion via Metal Halide Perovskite Solar-Driven Electrocatalysis. Journal of Physical Chemistry Letters, 2022, 13, 25-41.	4.6	10
10	AuPd nanoparticle-decorated ultrathin Bi ₂ TiO ₄ F ₂ sheets for photocatalytic methane oxidation. New Journal of Chemistry, 2022, 46, 10545-10549.	2.8	1
11	Site ensitive Selective CO ₂ Photoreduction to CO over Gold Nanoparticles. Angewandte Chemie - International Edition, 2022, 61, e202204563.	13.8	33
12	Site‧ensitive Selective CO ₂ Photoreduction to CO over Gold Nanoparticles. Angewandte Chemie, 2022, 134, .	2.0	5
13	Lamellar MXene Nanofiltration Membranes for Electrostatic Modulation of Molecular Permeation: Implications for Fine Separation. ACS Applied Nano Materials, 2022, 5, 7373-7381.	5.0	9
14	Intimately Contacted Ni2P on CdS Nanorods for Highly Efficient Photocatalytic H2 Evolution: New Phosphidation Route and the Interfacial Separation Mechanism of Charge Carriers. Applied Catalysis B: Environmental, 2021, 281, 119443.	20.2	90
15	Electricâ€Fieldâ€Mediated Electron Tunneling of Supramolecular Naphthalimide Nanostructures for Biomimetic H ₂ Production. Angewandte Chemie - International Edition, 2021, 60, 1235-1243.	13.8	33
16	Electricâ€Fieldâ€Mediated Electron Tunneling of Supramolecular Naphthalimide Nanostructures for Biomimetic H 2 Production. Angewandte Chemie, 2021, 133, 1255-1263.	2.0	6
17	Tunable linear donor–Ĩ€â€"acceptor conjugated polymers with a vinylene linkage for visible-light driven hydrogen evolution. Catalysis Science and Technology, 2021, 11, 4021-4025.	4.1	16
18	Enhanced bacterial disinfection by Cul–BiOI/rGO hydrogel under visible light irradiation. RSC Advances, 2021, 11, 20446-20456.	3.6	11

JINLIN LONG

#	Article	IF	CITATIONS
19	Photoelectrochemical reduction of carbon dioxide. , 2021, , 197-210.		0
20	Highly Efficient Plasmon Induced Hot-Electron Transfer at Ag/TiO ₂ Interface. ACS Photonics, 2021, 8, 1497-1504.	6.6	30
21	Metallic Pt and PtO ₂ Dual-Cocatalyst-Loaded Binary Composite RGO-CN <i>_x</i> for the Photocatalytic Production of Hydrogen and Hydrogen Peroxide. ACS Sustainable Chemistry and Engineering, 2021, 9, 6380-6389.	6.7	29
22	Activation of Carbonyl Oxygen Sites in βâ€Ketoenamineâ€Linked Covalent Organic Frameworks via Cyano Conjugation for Efficient Photocatalytic Hydrogen Evolution. Small, 2021, 17, e2101017.	10.0	34
23	The Hole‶unneling Heterojunction of Hematiteâ€Based Photoanodes Accelerates Photosynthetic Reaction. Angewandte Chemie - International Edition, 2021, 60, 16009-16018.	13.8	37
24	The Holeâ€Tunneling Heterojunction of Hematiteâ€Based Photoanodes Accelerates Photosynthetic Reaction. Angewandte Chemie, 2021, 133, 16145-16154.	2.0	2
25	Crystalline Covalent Organic Frameworks with Tailored Linkages for Photocatalytic H ₂ Evolution. ChemSusChem, 2021, 14, 4958-4972.	6.8	56
26	Conversion of CO2 to formic acid by integrated all-solar-driven artificial photosynthetic system. Journal of Power Sources, 2021, 512, 230532.	7.8	21
27	All-solid-state direct Z-scheme NiTiO ₃ /Cd _{0.5} Zn _{0.5} S heterostructures for photocatalytic hydrogen evolution with visible light. Journal of Materials Chemistry A, 2021, 9, 10270-10276.	10.3	136
28	Subsurface Defect Engineering in Single-Unit-Cell Bi ₂ WO ₆ Monolayers Boosts Solar-Driven Photocatalytic Performance. ACS Catalysis, 2020, 10, 1439-1443.	11.2	138
29	Molecular Engineering of Fully Conjugated sp ² Carbonâ€Linked Polymers for Highâ€Efficiency Photocatalytic Hydrogen Evolution. ChemSusChem, 2020, 13, 672-676.	6.8	26
30	Tuning Intermediate-Band Cu ₃ VS ₄ Nanocrystals from Plasmonic-like to Excitonic via Shell-Coating. Chemistry of Materials, 2020, 32, 224-233.	6.7	13
31	Direct Z-Scheme Heterojunction of Semicoherent FAPbBr ₃ /Bi ₂ WO ₆ Interface for Photoredox Reaction with Large Driving Force. ACS Nano, 2020, 14, 16689-16697.	14.6	167
32	Integrating single Ni sites into biomimetic networks of covalent organic frameworks for selective photoreduction of CO ₂ . Chemical Science, 2020, 11, 6915-6922.	7.4	78
33	Plasmonic Electronsâ€Driven Solarâ€ŧoâ€Hydrocarbon Conversion over Au NR@ZnO Core‧hell Nanostructures. ChemCatChem, 2020, 12, 2989-2994.	3.7	12
34	Understanding structure-function relationships in HZSM-5 zeolite catalysts for photocatalytic oxidation of isopropyl alcohol. Journal of Catalysis, 2019, 377, 322-331.	6.2	21
35	Efficient Photothermal CO2 Methanation over RuO2/SrTiO3. Trends in Chemistry, 2019, 1, 459-460.	8.5	13
36	Hot Ï€â€Electron Tunneling of Metal–Insulator–COF Nanostructures for Efficient Hydrogen Production. Angewandte Chemie - International Edition, 2019, 58, 18290-18294.	13.8	138

#	Article	IF	CITATIONS
37	Gold Plasmonâ€Enhanced Solar Hydrogen Production over SrTiO ₃ /TiO ₂ Heterostructures. ChemCatChem, 2019, 11, 6203-6207.	3.7	29
38	Hot Ï€â€Electron Tunneling of Metal–Insulator–COF Nanostructures for Efficient Hydrogen Production. Angewandte Chemie, 2019, 131, 18458-18462.	2.0	31
39	One-step green conversion of benzyl bromide to aldehydes on NaOH-modified g-C ₃ N ₄ with dioxygen under LED visible light. Catalysis Science and Technology, 2019, 9, 3270-3278.	4.1	15
40	<i>In situ</i> construction of layered graphene-based nanofiltration membranes with interlayer photocatalytic purification function and their application for water treatment. Environmental Science: Nano, 2019, 6, 2195-2202.	4.3	10
41	Synthesis of caged iodine-modified ZnO nanomaterials and study on their visible light photocatalytic antibacterial properties. Applied Catalysis B: Environmental, 2019, 256, 117873.	20.2	79
42	Plasmonic control of solar-driven CO2 conversion at the metal/ZnO interfaces. Applied Catalysis B: Environmental, 2019, 256, 117823.	20.2	95
43	Defect engineering of metal–oxide interface for proximity of photooxidation and photoreduction. Proceedings of the National Academy of Sciences of the United States of America, 2019, 116, 10232-10237.	7.1	63
44	Highâ€Rate, Tunable Syngas Production with Artificial Photosynthetic Cells. Angewandte Chemie, 2019, 131, 7800-7804.	2.0	12
45	Highâ€Rate, Tunable Syngas Production with Artificial Photosynthetic Cells. Angewandte Chemie - International Edition, 2019, 58, 7718-7722.	13.8	75
46	Reconstructing Dualâ€Induced {0 0 1} Facets Bismuth Oxychloride Nanosheets Heterostructures: An Effective Strategy to Promote Photocatalytic Oxygen Evolution. Solar Rrl, 2019, 3, 1900059.	5.8	44
47	3D flower-like heterostructured TiO2@Ni(OH)2 microspheres for solar photocatalytic hydrogen production. Chinese Journal of Catalysis, 2019, 40, 320-325.	14.0	49
48	Z-Schemed WO3/rGO/SnIn4S8 Sandwich Nanohybrids for Efficient Visible Light Photocatalytic Water Purification. Catalysts, 2019, 9, 187.	3.5	23
49	C(sp ³)–H Bond Activation by Perovskite Solar Photocatalyst Cell. ACS Energy Letters, 2019, 4, 203-208.	17.4	114
50	Heterogeneous Photocatalyzed Câ^'C Crossâ€coupling Reactions Under Visibleâ€light and Nearâ€infrared Light Irradiation. ChemCatChem, 2019, 11, 669-683.	3.7	41
51	Amorphous Ta2OxNy-enwrapped TiO2 rutile nanorods for enhanced solar photoelectrochemical water splitting. Applied Catalysis B: Environmental, 2019, 243, 481-489.	20.2	86
52	Pyrochlore Pr2Zr1.95In0.05O7+l̂´oxygen conductors: Defect-induced electron transport and enhanced NO2 sensing performances. Electrochimica Acta, 2019, 293, 338-347.	5.2	16
53	Efficient and Selective Photocatalytic Oxidation of Benzylic Alcohols with Hybrid Organic–Inorganic Perovskite Materials. ACS Energy Letters, 2018, 3, 755-759.	17.4	222
54	Green synthesis of red-emission carbon based dots by microbial fermentation. New Journal of Chemistry, 2018, 42, 8591-8595.	2.8	8

#	Article	IF	CITATIONS
55	Reducing the barrier effect of graphene sheets on a Ag cocatalyst to further improve the photocatalytic performance of TiO ₂ . RSC Advances, 2018, 8, 14056-14063.	3.6	7
56	Gold plasmon-induced photocatalytic dehydrogenative coupling of methane to ethane on polar oxide surfaces. Energy and Environmental Science, 2018, 11, 294-298.	30.8	202
57	Reduced Graphene Oxideâ€Cadmium Sulfide Nanorods Decorated with Silver Nanoparticles for Efficient Photocatalytic Reduction Carbon Dioxide Under Visible Light. ChemCatChem, 2018, 10, 1627-1634.	3.7	63
58	Amorphous NiO as co-catalyst for enhanced visible-light-driven hydrogen generation over g-C 3 N 4 photocatalyst. Applied Catalysis B: Environmental, 2018, 222, 35-43.	20.2	252
59	Visible-Light Driven Overall Conversion of CO ₂ and H ₂ O to CH ₄ and O ₂ on 3D-SiC@2D-MoS ₂ Heterostructure. Journal of the American Chemical Society, 2018, 140, 14595-14598.	13.7	361
60	Optofluidic Tunable Lenses for In-Plane Light Manipulation. Micromachines, 2018, 9, 97.	2.9	22
61	Cul-BiOl/Cu film for enhanced photo-induced charge separation and visible-light antibacterial activity. Applied Catalysis B: Environmental, 2018, 235, 238-245.	20.2	85
62	Pyrochlore Pr2Zr2-xMxO7+Î′ (M =†Al, Ga, In) solid-state electrolytes: Defect-mediated oxygen hopping pathways and enhanced NO2 sensing properties. Sensors and Actuators B: Chemical, 2018, 270, 130-139.	7.8	23
63	A graphene-hidden structure with diminished light shielding effect: more efficient graphene-involved composite photocatalysts. Catalysis Science and Technology, 2018, 8, 4734-4740.	4.1	24
64	Smallâ€&ized Bimetallic CuPd Nanoclusters Encapsulated Inside Cavity of NH ₂ â€UiOâ€66(Zr) with Superior Performance for Lightâ€Induced Suzuki Coupling Reaction. Small Methods, 2018, 2, 1800164.	8.6	59
65	Cd3(C3N3S3)2 coordination polymer/graphene nanoarchitectures for enhanced photocatalytic H2O2 production under visible light. Science Bulletin, 2017, 62, 610-618.	9.0	55
66	Ce incorporated pyrochlore Pr2Zr2O7 solid electrolytes for enhanced mild-temperature NO2 sensing. Ceramics International, 2017, 43, 11799-11806.	4.8	24
67	Molecular p–n heterojunction-enhanced visible-light hydrogen evolution over a N-doped TiO ₂ photocatalyst. Catalysis Science and Technology, 2017, 7, 2039-2049.	4.1	27
68	Metal-Free Photocatalysts C ₃ N ₃ S ₃ and its Polymers: Solubility in Water and Application in Benzylic Alcohols Oxidation Under Visible Light. Nano, 2017, 12, 1750101.	1.0	3
69	Graphitic carbon/carbon nitride hybrid as metal-free photocatalyst for enhancing hydrogen evolution. Applied Catalysis A: General, 2017, 546, 30-35.	4.3	27
70	Compact carbon nitride based copolymer films with controllable thickness for photoelectrochemical water splitting. Journal of Materials Chemistry A, 2017, 5, 19062-19071.	10.3	43
71	Alkaline-Earth Metals-Doped Pyrochlore Gd2Zr2O7 as Oxygen Conductors for Improved NO2 Sensing Performance. Scientific Reports, 2017, 7, 4684.	3.3	36
72	Dual couples Bi metal depositing and Ag@AgI islanding on BiOI 3D architectures for synergistic bactericidal mechanism of E. coli under visible light. Applied Catalysis B: Environmental, 2017, 204, 1-10.	20.2	156

#	Article	IF	CITATIONS
73	Post-synthetic regulation of the structure, morphology and photoactivity of graphitic carbon nitride by heat-vacuum treatment. Materials and Design, 2017, 114, 208-213.	7.0	7
74	Q-switching Yb^3+: YAG lasers based on plasmon resonance nonlinearities of Cu_2â^'xSe@Cu_2â^'xS nanorods. Optics Letters, 2017, 42, 2619.	3.3	1
75	A Longâ€Lived Mononuclear Cyclopentadienyl Ruthenium Complex Grafted onto Anatase TiO ₂ for Efficient CO ₂ Photoreduction. Angewandte Chemie, 2016, 128, 8454-8458.	2.0	80
76	A Longâ€Lived Mononuclear Cyclopentadienyl Ruthenium Complex Grafted onto Anatase TiO ₂ for Efficient CO ₂ Photoreduction. Angewandte Chemie - International Edition, 2016, 55, 8314-8318.	13.8	96
77	Synergy of metal and nonmetal dopants for visible-light photocatalysis: a case-study of Sn and N co-doped TiO ₂ . Physical Chemistry Chemical Physics, 2016, 18, 9636-9644.	2.8	68
78	I-TiO2/PVC film with highly photocatalytic antibacterial activity under visible light. Colloids and Surfaces B: Biointerfaces, 2016, 144, 196-202.	5.0	26
79	Structural evolution of alkaline earth metal stannates MSnO ₃ (M = Ca, Sr, and Ba) photocatalysts for hydrogen production. RSC Advances, 2016, 6, 42474-42481.	3.6	78
80	One-step synthesis of mesoporous Pt–Nb ₂ O ₅ nanocomposites with enhanced photocatalytic hydrogen production activity. RSC Advances, 2016, 6, 96809-96815.	3.6	20
81	Large-scale preparation of heterometallic chalcogenide MnSb ₂ S ₄ monolayer nanosheets with a high visible-light photocatalytic activity for H ₂ evolution. Chemical Communications, 2016, 52, 13381-13384.	4.1	18
82	One-pot fabrication of Bi3O4Cl/BiOCl plate-on-plate heterojunction with enhanced visible-light photocatalytic activity. Applied Catalysis B: Environmental, 2016, 185, 203-212.	20.2	141
83	Robust Photocatalytic H2O2 Production by Octahedral Cd3(C3N3S3)2 Coordination Polymer under Visible Light. Scientific Reports, 2015, 5, 16947.	3.3	71
84	Interim Anatase Coating Layer Stabilizes Rutile@Cr _{<i>x</i>} O _{<i>y</i>} Photoanode for Visibleâ€Lightâ€Driven Water Oxidation. ChemPhysChem, 2015, 16, 1352-1355.	2.1	8
85	Hydrothermal synthesis of MSn(OH)6 (M = Co, Cu, Fe, Mg, Mn, Zn) and their photocatalytic activity for the destruction of gaseous benzene. Chemical Engineering Journal, 2015, 269, 168-179.	12.7	45
86	Photocatalytic reduction of CO ₂ with H ₂ O to CH ₄ on Cu(<scp>i</scp>) supported TiO ₂ nanosheets with defective {001} facets. Physical Chemistry Chemical Physics, 2015, 17, 9761-9770.	2.8	110
87	Heteroatomic Ni, Sn Clusters-Grafted Anatase TiO ₂ Photocatalysts: Structure, Electron Delocalization, and Synergy for Solar Hydrogen Production. Journal of Physical Chemistry C, 2015, 119, 10478-10492.	3.1	35
88	lodine-modified nanocrystalline titania for photo-catalytic antibacterial application under visible light illumination. Applied Catalysis B: Environmental, 2015, 176-177, 36-43.	20.2	62
89	Towards a comprehensive insight into efficient hydrogen production by self-assembled Ru(bpy) ₃ ²⁺ –polymer–Pt artificial photosystems. Physical Chemistry Chemical Physics, 2015, 17, 10726-10736.	2.8	15
90	Layered metal–organic framework/graphene nanoarchitectures for organic photosynthesis under visible light. Journal of Materials Chemistry A, 2015, 3, 24261-24271.	10.3	130

#	Article	IF	CITATIONS
91	Monolayered Bi2WO6 nanosheets mimicking heterojunction interface with open surfaces for photocatalysis. Nature Communications, 2015, 6, 8340.	12.8	578
92	Template-free synthesis of porous graphitic carbon nitride microspheres for enhanced photocatalytic hydrogen generation with high stability. Applied Catalysis B: Environmental, 2015, 165, 503-510.	20.2	207
93	Gold-plasmon enhanced solar-to-hydrogen conversion on the {001} facets of anatase TiO2 nanosheets. Energy and Environmental Science, 2014, 7, 973.	30.8	159
94	Single-site nickel-grafted anatase TiO 2 for hydrogen production: Toward understanding the nature of visible-light photocatalysis. Journal of Catalysis, 2014, 320, 147-159.	6.2	67
95	Vacuum heat-treatment of carbon nitride for enhancing photocatalytic hydrogen evolution. Journal of Materials Chemistry A, 2014, 2, 17797-17807.	10.3	94
96	Visible light-driven decomposition of gaseous benzene on robust Sn ²⁺ -doped anatase TiO ₂ nanoparticles. RSC Advances, 2014, 4, 34315-34324.	3.6	44
97	Fabrication of robust M/Ag ₃ PO ₄ (M = Pt, Pd, Au) Schottky-type heterostructures for improved visible-light photocatalysis. RSC Advances, 2014, 4, 37220.	3.6	64
98	Layered C ₃ N ₃ S ₃ Polymer/Graphene Hybrids as Metal-Free Catalysts for Selective Photocatalytic Oxidation of Benzylic Alcohols under Visible Light. ACS Catalysis, 2014, 4, 3302-3306.	11.2	89
99	Bi ₂ MoO ₆ Nanobelts for Crystal Facetâ€Enhanced Photocatalysis. Small, 2014, 10, 2791-2795.	10.0	145
100	Ternary Pt/SnOx/TiO2 photocatalysts for hydrogen production: consequence of Pt sites for synergy of dual co-catalysts. Physical Chemistry Chemical Physics, 2014, 16, 12521.	2.8	65
101	Visible-light photocatalytic denitrogenation of nitrogen-containing compound in petroleum by metastable Bi20TiO32. International Journal of Hydrogen Energy, 2014, 39, 13401-13407.	7.1	23
102	Au deposited BiOCl with different facets: On determination of the facet-induced transfer preference of charge carriers and the different plasmonic activity. Applied Catalysis B: Environmental, 2014, 160-161, 98-105.	20.2	75
103	Self-assembled micro/nano-structured Zn2GeO4 hollow spheres: direct synthesis and enhanced photocatalytic activity. Journal of Materials Chemistry A, 2013, 1, 10622.	10.3	26
104	Single-site Sn-grafted Ru/TiO2 photocatalysts for biomass reforming: Synergistic effect of dual co-catalysts and molecular mechanism. Journal of Catalysis, 2013, 303, 141-155.	6.2	89
105	Enhanced Hydrogen Production over C-Doped CdO Photocatalyst in NaS/NaSO Solution under Visible Light Irradiation. International Journal of Photoenergy, 2012, 2012, 1-7.	2.5	11
106	Amine-functionalized zirconium metal–organic framework as efficient visible-light photocatalyst for aerobic organic transformations. Chemical Communications, 2012, 48, 11656.	4.1	405
107	Nitrogen-doped graphene stabilized gold nanoparticles for aerobic selective oxidation of benzylic alcohols. RSC Advances, 2012, 2, 12438.	3.6	84
108	Visible light-induced highly efficient organic pollutant degradation and concomitant CO2 fixation using red lead. RSC Advances, 2012, 2, 12624.	3.6	8

#	Article	IF	CITATIONS
109	Photoinduced Reactions between Pb ₃ O ₄ and Organic Dyes in Aqueous Solution under Visible Light. Inorganic Chemistry, 2012, 51, 12594-12596.	4.0	12
110	Nitrogen-Doped Graphene Nanosheets as Metal-Free Catalysts for Aerobic Selective Oxidation of Benzylic Alcohols. ACS Catalysis, 2012, 2, 622-631.	11.2	384
111	In situ IR study of surface hydroxyl species of dehydrated TiO2: towards understanding pivotal surface processes of TiO2 photocatalytic oxidation of toluene. Physical Chemistry Chemical Physics, 2012, 14, 9468.	2.8	127
112	Probing the Electronic Structure and Photoactivation Process of Nitrogenâ€Doped TiO ₂ Using DRS, PL, and EPR. ChemPhysChem, 2012, 13, 1542-1550.	2.1	29
113	Controlling the synergistic effect of oxygen vacancies and N dopants to enhance photocatalytic activity of N-doped TiO2 by H2 reduction. Applied Catalysis A: General, 2012, 425-426, 117-124.	4.3	76
114	Single-site tin-grafted anatase TiO2 for photocatalytic hydrogen production: Toward understanding the nature of interfacial molecular junctions formed in semiconducting composite photocatalysts. Journal of Catalysis, 2012, 289, 88-99.	6.2	49
115	Organic semiconductor for artificial photosynthesis: water splitting into hydrogen by a bioinspired C ₃ N ₃ S ₃ polymer under visible light irradiation. Chemical Science, 2011, 2, 1826-1830.	7.4	167
116	Surface Chlorination of TiO ₂ -Based Photocatalysts: A Way to Remarkably Improve Photocatalytic Activity in Both UV and Visible Region. ACS Catalysis, 2011, 1, 200-206.	11.2	71
117	Sn2+ dopant induced visible-light activity of SnO2 nanoparticles for H2 production. Catalysis Communications, 2011, 16, 215-219.	3.3	64
118	Trinuclear iron cluster intercalated montmorillonite catalyst: Microstructure and photo-Fenton performance. Catalysis Today, 2011, 175, 362-369.	4.4	16
119	Nitrogen-doped titanium dioxide visible light photocatalyst: Spectroscopic identification of photoactive centers. Journal of Catalysis, 2010, 276, 201-214.	6.2	185
120	H2–O2 promoting effect on photocatalytic degradation of organic pollutants in an aqueous solution without an external H2 supply. Applied Catalysis A: General, 2010, 380, 178-184.	4.3	8
121	Efficient Photocatalytic Degradation of Volatile Organic Compounds by Porous Indium Hydroxide Nanocrystals. Environmental Science & Technology, 2010, 44, 1380-1385.	10.0	96
122	Catalytic Role of Cu Sites of Cu/MCM-41 in Phenol Hydroxylation. Langmuir, 2010, 26, 1362-1371.	3.5	80
123	Infrared Study of the NO Reduction by Hydrocarbons over Iron Sites with Low Nuclearity: Some New Insight into the Reaction Pathway. Journal of Physical Chemistry C, 2010, 114, 15713-15727.	3.1	28
124	Binuclear μ-hydroxo-bridged iron clusters derived from surface organometallic chemistry of ferrocene in cavities of HY zeolite: Local structure, bound sites, and catalytic reactivity. Journal of Catalysis, 2009, 264, 163-174.	6.2	23
125	Photochemical synthesis of submicron- and nano-scale Cu2O particles. Journal of Colloid and Interface Science, 2009, 333, 791-799.	9.4	41
126	Hydrothermal synthesis, characterization, and photocatalytic properties of Zn2SnO4. Journal of Solid State Chemistry, 2009, 182, 517-524.	2.9	108

#	Article	IF	CITATIONS
127	Hydroxide ZnSn(OH)6: A promising new photocatalyst for benzene degradation. Applied Catalysis B: Environmental, 2009, 91, 67-72.	20.2	122
128	Controlled synthesis of pure and highly dispersive Cu(ii), Cu(i), and Cu(0)/MCM-41 with Cu[OCHMeCH2NMe2]2/MCM-41 as precursor. New Journal of Chemistry, 2009, 33, 2044.	2.8	33
129	Photocatalytic and antibacterial properties of medicalâ€grade PVC material coated with TiO ₂ film. Journal of Biomedical Materials Research - Part B Applied Biomaterials, 2008, 87B, 425-431.	3.4	54
130	Urea-based hydrothermal growth, optical and photocatalytic properties of single-crystalline In(OH)3 nanocubes. Journal of Colloid and Interface Science, 2008, 325, 425-431.	9.4	75
131	Indium hydroxide: A highly active and low deactivated catalyst for photoinduced oxidation of benzene. Comptes Rendus Chimie, 2008, 11, 101-106.	0.5	55
132	Photoactive sites in commercial HZSM-5 zeolite with iron impurities: An UV Raman study. Comptes Rendus Chimie, 2008, 11, 114-119.	0.5	7
133	Photocatalytic reforming of biomass: A systematic study of hydrogen evolution from glucose solution. International Journal of Hydrogen Energy, 2008, 33, 6484-6491.	7.1	301
134	Construction of highly dispersed mononuclear iron-oxo species in the supercages of Y zeolite by use of surface organometallic chemistry. Microporous and Mesoporous Materials, 2008, 108, 258-265.	4.4	15
135	Cyclopentadiene transformation over H-form zeolites: TPD and IR studies of the formation of a monomeric cyclopentenyl carbenium ion intermediate and its role in acid-catalyzed conversions. Journal of Catalysis, 2008, 255, 48-58.	6.2	20
136	Controlled preparation of In2O3, InOOH and In(OH)3via a one-pot aqueous solvothermal route. New Journal of Chemistry, 2008, 32, 1843.	2.8	39
137	Deposition Chemistry of Cu[OCH(Me)CH ₂ NMe ₂] ₂ over Mesoporous Silica. Chemistry of Materials, 2008, 20, 4565-4575.	6.7	16
138	Insight into Photoactive Sites for the Ethylene Oxidation on Commercial HZSM-5 Zeolites with Iron Impurities by UV Raman, X-ray Absorption Fine Structure, and Electron Paramagnetic Resonance Spectroscopies. Journal of Physical Chemistry C, 2007, 111, 5195-5202.	3.1	10
139	A Mononuclear Cyclopentadiene–Iron Complex Grafted in the Supercages of HY Zeolite: Synthesis, Structure, and Reactivity. Chemistry - A European Journal, 2007, 13, 7890-7899.	3.3	23